Towards modeling boundary layer transition in large-eddy simulations

By M. J. P. Hack AND P. Moin

1. Motivation and objectives

The modeling of the laminar region and the prediction of transition remain key challenges in the simulation of external aerodynamic flows. The issue is of particular relevance for wall-modeled large eddy simulations (WMLES) which must allot 10 to 100 times more grid points than used in the turbulent regime just to resolve the growth of small disturbances in the thin laminar region (Slotnick *et al.* 2014). The present study examines the potential of the parabolized stability equations (PSE) to provide an accurate yet computationally efficient treatment of the pre-transitional flow regime.

Boundary-layer transition is often preceded by the growth of initially small disturbances inside the shear. Over a range of Reynolds numbers, the profile of the Blasius flat-plate boundary layer supports the exponential growth of a two-dimensional instability known as Tollmien-Schlichting (TS) wave. Once its amplitude is on the order of one percent of the the free-stream convective velocity, the TS wave begins to interact with three-dimensional disturbances. In K-type natural transition, the frequency of these three-dimensional disturbances matches the TS wave, while they are subharmonic in H-type transition to turbulence. The nonlinear interaction between the disturbances introduces new modes and rapidly broadens the spectrum. In flow visualizations, this process is accompanied by the formation of characteristic hairpin vortices. The statistics of late-stage transition begin to resemble developed turbulent boundary layers (Sayadi *et al.* 2013), albeit with a local skin-friction overshoot.

Sayadi & Moin (2012) conducted large eddy simulations (LES) of K- and H-type transitional boundary layers. They found that constant coefficient models for the subgrid scale stress tensor could not predict the rapid rise in skin friction at the onset of transition as the non-negligible turbulent viscosity in the laminar region dampens the amplification of instabilities. Dynamic models sufficiently reduced the turbulent viscosity in the laminar flow to allow the growth of disturbances. When the grid was fine enough, the LES reproduced the skin-friction overshoot observed in DNS.

Park & Moin (2014) applied WMLES based on a dynamic non-equilibrium wall model to the subharmonic transition scenario studied among others by Kachanov & Levchenko (1984) and Sayadi *et al.* (2013). The number of grid points used in the WMLES was several hundred times lower than that of direct simulations. However, in order to resolve the exponential instabilities in the laminar portion of the boundary layer through the onset of transition, the wall-model had to be deactivated and a fine grid was required. The fine resolution in that region restricted the time step of the entire simulation and hence the overall computational cost. The conclusion is that while WMLES is a useful tool for fully turbulent flows, it is inadequate in the laminar region. A recent NASA report accordingly described the efficient yet accurate treatment of the laminar region and the reliable prediction of the onset of transition as one of the key impediments in the current state of CFD technology (Slotnick *et al.* 2014).

The present study aims to combine the individual advantages of the PSE and WMLES approaches to enable the accurate and reliable prediction of boundary layer transition. In the laminar regime, the streamwise evolution of the instability waves is captured using the nonlinear form of the PSE. Once the flow begins to transition, the local PSE solution is used as the inflow boundary condition of a wall-modeled large eddy simulation.

2. Parabolized stability equations

The PSE were introduced by Herbert (1991) and Bertolotti *et al.* (1992) as a computationally efficient alternative to direct numerical simulations in the study of convectively unstable flows such as laminar boundary layers. The PSE can incorporate both nonparallel and nonlinear effects and thus capture the flow physics more faithfully than classical stability theory based on the assumption of parallel flow. Comparisons of the amplification of instabilities in boundary layers between PSE and DNS by Bertolotti *et al.* (1992) and Joslin *et al.* (1993) showed excellent agreement.

The derivation of the PSE for incompressible flow starts by decomposing the state vector, $\boldsymbol{Q} = (U, V, W, P)^{\mathsf{T}}$, into a base state and a perturbation component, $\boldsymbol{Q}(x, y, z, t) = \bar{\boldsymbol{q}}(x, y) + \boldsymbol{q}(x, y, z, t)$. Introduction of this decomposition into the Navier-Stokes equations and subtraction of mean-flow terms yields

$$\frac{\partial \boldsymbol{u}}{\partial t} + \boldsymbol{U} \cdot \boldsymbol{\nabla} \boldsymbol{u} + \boldsymbol{u} \cdot \boldsymbol{\nabla} \boldsymbol{U} + \frac{1}{\rho} \boldsymbol{\nabla} p - \frac{1}{Re} \Delta \boldsymbol{u} = -\boldsymbol{u} \cdot \boldsymbol{\nabla} \boldsymbol{u}, \tag{2.1}$$

$$\boldsymbol{\nabla} \cdot \boldsymbol{u} = 0. \tag{2.2}$$

In the following, the perturbation field is assumed periodic in the spanwise dimension and time and is expressed in terms of a Fourier expansion. The streamwise variation of the disturbance is split into a fast-changing oscillatory component that is governed by a complex wavenumber, $\alpha(x)$, and a slowly changing shape function, $\hat{\boldsymbol{q}}(x, y)$. The full ansatz for the disturbance field thus becomes

$$\boldsymbol{q}(x, y, z, t) = \sum_{n=-N}^{N} \sum_{m=-M}^{M} \hat{\boldsymbol{q}}_{n,m}(x, y) \exp\left(\mathrm{i} \int_0^x \alpha_{n,m}(\xi)\, \mathrm{d}\xi + \mathrm{i} n \beta z - \mathrm{i} m \omega t \right), \tag{2.3}$$

where β is the real spanwise wavenumber of the disturbance and ω is its real frequency. All lengths are normalized by the boundary layer thickness at the inflow location x_0 of the computational domain and velocities are normalized by the free-stream convective speed at that location. The spanwise and temporal Fourier expansions are truncated at a finite number of N and M modes, respectively. The ambiguity arising from the streamwise variation of both $\hat{\boldsymbol{q}}$ and α is resolved via the constraint

$$\int_{\Omega_y} \hat{\boldsymbol{q}}_{n,m}^{\mathsf{H}} \frac{\partial \hat{\boldsymbol{q}}_{n,m}}{\partial x}\, \mathrm{d}y = 0, \tag{2.4}$$

which ensures that the $\hat{\boldsymbol{q}}_{n,m}(x, y)$ only weakly depend on the streamwise coordinate. Introducing the ansatz Eq. (2.3) and retaining terms up to order $\mathcal{O}\left(Re^{-1}\right)$, the parabolized stability equations take the form

$$\mathsf{A} \hat{\boldsymbol{q}}_{n,m} + \mathsf{B} \frac{\partial \hat{\boldsymbol{q}}_{n,m}}{\partial y} + \mathsf{C} \frac{\partial^2 \hat{\boldsymbol{q}}_{n,m}}{\partial y^2} + \mathsf{D} \frac{\partial \hat{\boldsymbol{q}}_{n,m}}{\partial x} = \hat{\boldsymbol{F}}_{n,m}. \tag{2.5}$$

The definitions of the operators A, B, C and D for a steady, three-dimensional base state

$\boldsymbol{U} = (U, V, W)^{\mathsf{T}}$ are

$$\mathsf{A} = \begin{pmatrix} r + \frac{\partial U}{\partial x} & \frac{\partial U}{\partial y} & 0 & \mathrm{i}\alpha \\ 0 & r + \frac{\partial V}{\partial y} & 0 & 0 \\ \frac{\partial W}{\partial x} & \frac{\partial W}{\partial y} & r & \mathrm{i}\beta \\ \mathrm{i}\alpha & 0 & \mathrm{i}\beta & 0 \end{pmatrix} \qquad \mathsf{B} = \begin{pmatrix} V & 0 & 0 & 0 \\ 0 & V & 0 & 1 \\ 0 & 0 & V & 0 \\ 0 & 1 & 0 & 0 \end{pmatrix}$$

$$\mathsf{C} = \begin{pmatrix} -\frac{1}{Re} & 0 & 0 & 0 \\ 0 & -\frac{1}{Re} & 0 & 0 \\ 0 & 0 & -\frac{1}{Re} & 0 \\ 0 & 0 & 0 & 0 \end{pmatrix} \qquad \mathsf{D} = \begin{pmatrix} U & 0 & 0 & 1 \\ 0 & U & 0 & 0 \\ 0 & 0 & U & 0 \\ 1 & 0 & 0 & 0 \end{pmatrix},$$

with $r = -\mathrm{i}m\omega + \mathrm{i}\alpha_{n,m}U + \mathrm{i}n\beta U + \frac{1}{Re}\left(\alpha_{n,m}^2 + n^2\beta^2\right)$. The forcing term $\hat{\boldsymbol{F}}_{n,m}$ accounts for the nonlinear terms on the right-hand side of Eq. (2.1) and is evaluated via a fast Fourier transform. In order to keep the computational effort at a minimum, the marching procedure at first only considers modes that are part of the initial condition. Additional modes are included if the magnitude of the respective nonlinear term, $\hat{\boldsymbol{F}}_{n,m}$, exceeds a threshold which is set to 10^{-7} in the present study.

Note that the above form Eq. (2.5) of the parabolized stability equations is not fully parabolic, which makes the system ill-posed for a spatial marching approach. Detailed analyses by Haj-Hariri (1994) showed that the streamwise pressure gradient is the main contributor to the residual ellipticity. Following Day *et al.* (2001), we alleviate this issue by introducing a damping factor $0 \leq \epsilon \leq 1$ such that

$$\frac{\partial p}{\partial x} = \sum_{m=-M}^{M} \sum_{n=-N}^{N} \left(\mathrm{i}\alpha_{n,m}\, \hat{p}_{n,m} + \epsilon \frac{\partial \hat{p}_{n,m}}{\partial x} \right) \exp\left[\mathrm{i}\left(n\beta z - m\omega t\right)\right]. \tag{2.6}$$

Even in the extreme case $\epsilon = 0$, this approach only removes the slow contribution to the total pressure gradient while the fast part associated with the harmonic oscillation and the exponential growth of the instability is retained.

Homogeneous Dirichlet boundary conditions are used for regular modes with $n \times m \neq 0$ both at the wall and in the free-stream

$$u_{n,m}, v_{n,m}, w_{n,m} = 0 \quad \text{at} \quad y = 0, \qquad u_{n,m}, v_{n,m}, w_{n,m} = 0 \quad \text{at} \quad y \to \infty. \tag{2.7}$$

In the case of the mean-flow distortion ($n = 0$, $m = 0$) mass conservation requires a non-zero wall-normal velocity in the free stream, so that

$$u_{0,0}, v_{0,0}, w_{0,0} = 0 \quad \text{at} \quad y = 0, \qquad u_{0,0}, \frac{\partial v_{0,0}}{\partial y}, w_{0,0} = 0 \quad \text{at} \quad y \to \infty. \tag{2.8}$$

A second-order backward discretization is used to advance the solution in x. The wall-normal discretization uses a spectral approach based on Chebyshev polynomials.

Several factors contribute to the increased computational efficiency of the PSE approach when compared to direct numerical simulations. First, the Fourier series in t and z, Eq. (2.3), is severely truncated. Furthermore, the decomposition of the streamwise derivative into a slow- and fast-changing part allows a coarser streamwise resolution since the grid only needs to resolve the former (cf. Section 3.). Finally, the parabolic nature of the equations permits their solution via an efficient marching procedure in x.

3. Grid point requirement

Choi & Moin (2012) investigated the grid point requirement in simulations of fully turbulent boundary layers. They showed that in wall-resolved LES, the number of grid points N is proportional to $Re_{L_x}^{13/7}$ grid points, where L_x is the streamwise extent of the flat plate. In wall-modeled LES, the grid point requirement reduces to $N \sim Re_{L_x}$. Slotnick *et al.* (2014) extended the analysis to account for the laminar region of the boundary layer. They concluded that in the WMLES of a NACA 0012 profile at a chord Reynolds number $Re_c = 10^7$, seventy times as many grid points are needed in the laminar regime as in the turbulent region of the boundary layer.

The decomposition of the streamwise derivative into a slow- and fast-changing part used in the PSE considerably reduces the required number of grid points. This aspect is briefly quantified in the following. In a general spatial discretization as used for instance in DNS or LES, the three-dimensional flow field must be resolved by the grid with sufficient accuracy. For a field of the form $\mathcal{G} = g(x,y)\exp(\mathrm{i}\alpha x)$, the grid needs to represent both the variation in the shape function g as well as the oscillatory component. In the specific case of a TS wave, the wavelength is on the order of the boundary layer thickness, $\lambda = 2\pi/\Re(\alpha) \approx \delta$. Assuming a grid spacing inversely proportional to the gradient of the field, the number of grid points in the streamwise dimension to resolve the oscillatory component becomes

$$\begin{aligned} N_{x,\mathrm{fast}} = \int_{x_0}^{x_1} \frac{1}{\Delta x_{\mathrm{fast}}}\,\mathrm{d}x = 2\pi \int_{x_0}^{x_1} \frac{n_D}{\lambda}\,\mathrm{d}x \approx 2\pi \int_{x_0}^{x_1} \frac{n_D}{x}\frac{x}{\delta}\,\mathrm{d}x = \frac{2\pi}{5}\int_{x_0}^{x_1} \frac{n_D}{\sqrt{x}}\sqrt{\frac{U_\infty}{\nu}}\,\mathrm{d}x \\ = \frac{4\pi}{5} n_D \sqrt{U_\infty/\nu}\left[x_1^{1/2} - x_0^{1/2}\right], \end{aligned} \tag{3.1}$$

where n_D is a constant that depends on the discretization scheme. In Eq. (3.1), the relation $\delta/x = 5Re_x^{-1/2}$ which is valid for laminar Blasius boundary layers, was used (see e.g., Schlichting & Gersten 2006).

The slow streamwise change in the shape function $g(x,y)$ can be assumed to scale with the variation of the base state. For a grid spacing chosen inversely proportional to the gradient, the number of points to resolve this variation is

$$N_{x,\mathrm{slow}} = \int_{x_0}^{x_1} \frac{1}{\Delta x_{\mathrm{slow}}}\,\mathrm{d}x = \frac{1}{\delta_0}\int_{x_0}^{x_1} n_D \frac{\partial \delta}{\partial x}\,\mathrm{d}x \tag{3.2}$$

$$= \frac{1}{\delta_0} n_D\left[\delta_1 - \delta_0\right] \tag{3.3}$$

$$= \frac{5}{\delta_0} n_D \sqrt{\nu/U_\infty}\left[x_1^{1/2} - x_0^{1/2}\right]. \tag{3.4}$$

The theoretical ratio between the grid point requirements of the slow and fast contribution is therefore

$$\frac{N_{x,\mathrm{fast}}}{N_{x,\mathrm{slow}}} = \frac{4\pi}{25}\frac{U_\infty \delta_0}{\nu} = \frac{4\pi}{25} Re_{\delta_0}. \tag{3.5}$$

Since generally $Re_{\delta_0} \gg 1$, the number of grid points needed to resolve the fast change in a conventional spatial discretization is significantly higher than that required to resolve the slow change under the particular decomposition used in the PSE.

The individual efficiency of the PSE and the WMLES in the laminar and turbulent regimes motivates a hybrid approach that combines the two methodologies and provides an accurate and at the same time efficient computational treatment of transitional bound-

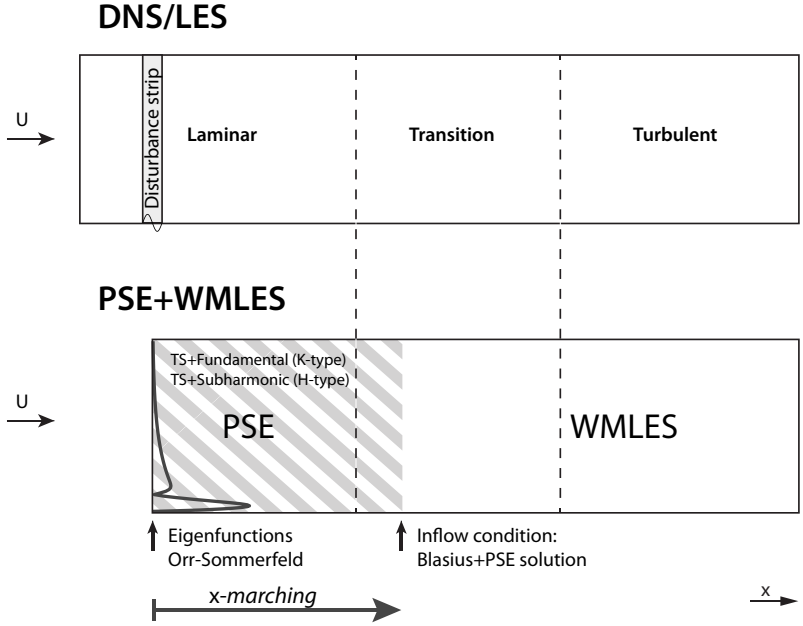

FIGURE 1. Top: Conventional approach to simulation of transitional flows used e.g. in the LES by Sayadi & Moin (2012) and the DNS by Sayadi *et al.* (2013). Bottom: Combination of PSE and WMLES approaches. At the onset of the transition region, the local PSE solution is used as the inflow condition of a wall-modeled large eddy simulation.

ary layers. Figure 1 compares the proposed approach to the conventional methodology of DNS or LES of transitional boundary layers. The initial condition of the PSE is taken from the local solution of the spatial Orr-Sommerfeld eigenvalue problem and is evolved up to the onset of transition region, where nonlinear effects become dominant and the PSE marching procedure commonly begins to diverge. The local solution at this position is prescribed as an inflow condition of the WMLES solver which covers the downstream remainder of the computational domain.

4. Application of the PSE to test cases

This Section provides a comparison of results obtained from the present implementation of the PSE with published data. It allows a verification of the implementation and an assessment of the capability of the PSE to identify the onset of transition to turbulence. The first considered case is the linear streamwise evolution of a two-dimensional TS wave ($\beta = 0$) with an initial amplitude of 0.25 percent and non-dimensional frequency $F = 10^6\omega\nu/U_\infty^2 = 86$. The marching extends from $Re_{\delta^*} = 400$ to $Re_{\delta^*} = 880$, where δ^* is the displacement thickness of the base flow. The initial shape function, $\hat{\boldsymbol{q}}\,(x = x_0, y)$ and streamwise wavenumber, $\alpha\,(x = x_0)$, are obtained from the solution of the spatial Orr-Sommerfeld/Squire problem at x_0. Nonlinear forcing terms in Eq. (2.5) are set to zero and the expansion contains one harmonic in the span ($N = 0$) and three harmonics in time ($M = 1$). The peak amplitude of the streamwise velocity component of the TS wave is provided by the dashed line Figure 2. The results are in excellent agreement with data from Bertolotti *et al.* (1992).

Nonlinear results are represented by the solid line in Figure 2. The initial amplitude and

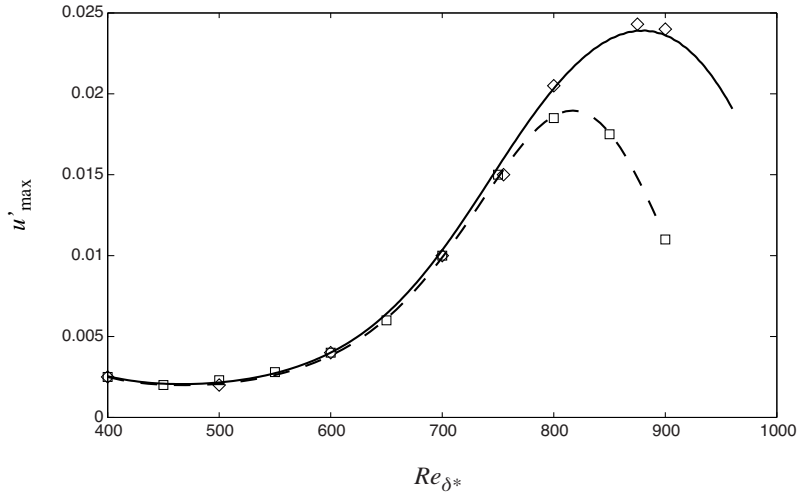

FIGURE 2. Amplitude of Tollmien-Schlichting waves at $F = 86$. Linear evolution (dashed) and nonlinear evolution (solid). Symbols show data from Bertolotti *et al.* (1992).

frequency are the same as in the linear case and eleven temporal harmonics are used ($M = 5$). Comparison with the linear case demonstrates that nonlinearity has an appreciable effect on the amplification of the TS wave, leading to an approximately 25 percent higher peak. A slight relative deviation of about two percent from the results of Bertolotti *et al.* (1992) is observed, which is possibly related to the different formulation based on a discretization of the streamfunction used in that work. For instance, Esfahanian *et al.* (2001) reported a comparable deviation from the data of Bertolotti *et al.* (1992) in the presence of nonlinear effects.

A second test case involves the subharmonic laminar-turbulent transition originally investigated by Herbert (1991) and more recently by Sayadi *et al.* (2013). In addition to a TS wave with frequency $2F = 124$, the solution at the initial position ($Re_{\delta^*} = 400$) includes a subharmonic mode with spanwise wavenumber $\beta = 0.15$. Following Kachanov & Levchenko (1984) and Herbert (1988), the initial amplitudes are 0.48 percent for the TS wave and 0.00145 percent for the subharmonic mode. The Fourier series contains 15 harmonics in time ($M = 7$) and seven harmonics in the spanwise dimension ($N = 3$). The main interest is whether the PSE can correctly identify the onset of transition, defined here as the streamwise minimum of the skin friction coefficient

$$C_f = \frac{\nu \frac{\partial U}{\partial y}|_{y=0}}{\frac{1}{2} U_\infty^2}.$$

The black line in Figure 3 provides the skin friction coefficient computed from the sum of the Blasius base flow and the mean-flow distortion, i.e. the $(0, 0)$ mode, taken from the PSE. The skin friction initially coincides with the laminar correlation and sharply rises at $Re_{\delta^*} \approx 1120$. Shortly after this point, the convergence of the PSE scheme deteriorates as the nonlinear forcing terms on the right-hand side of Eq. (2.5) begin to dominate. The insert in Figure 3 provides the skin-friction coefficient from the DNS by Sayadi *et al.* (2013). The minimum of the curve is located near $Re_{\delta^*} \approx 1100$, which demonstrates that the PSE can correctly identify the onset of the transitional region.

Finally, the amplitudes of individual modes in the H-type transition case are consid-

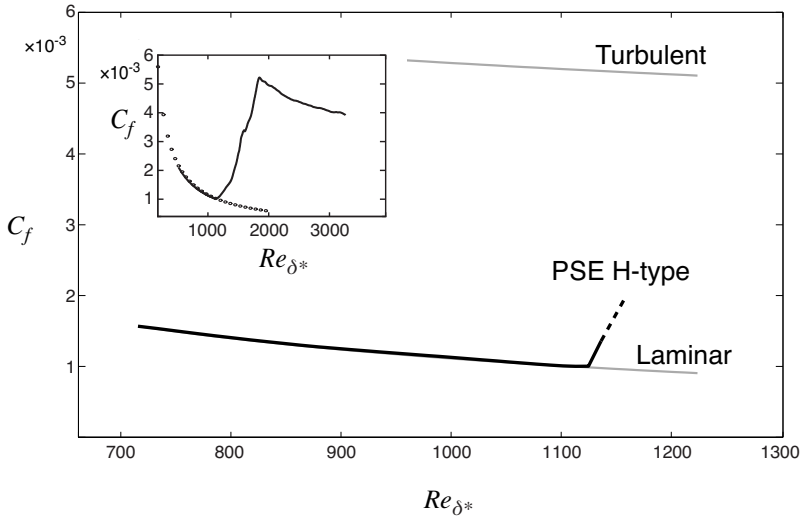

FIGURE 3. Skin friction coefficient for H-type transition. The insert shows results from Sayadi *et al.* (2013).

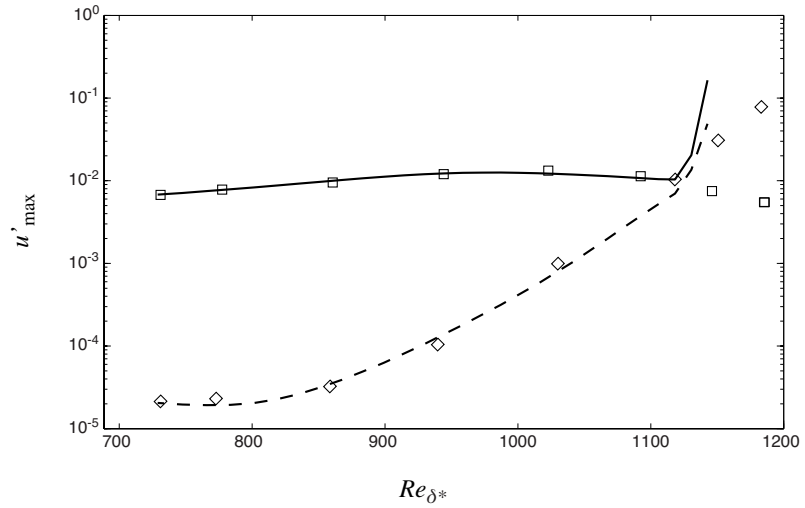

FIGURE 4. Amplitudes of TS wave (solid) and subharmonic mode (dashed) in H-type transition. Symbols indicate results from linear theory by Herbert (1988).

ered. Figure 4 presents the amplitude of the TS wave, i.e. the $(2, 0)$ mode, and the subharmonic $(1, 1)$ mode. While the TS wave grows moderately over the considered range, the subharmonic mode amplifies by several orders of magnitude. Results obtained by Herbert (1988) in a linear Floquet analysis based on a parallel-flow assumption are included as symbols. Initially, the two sets of results are in good agreement. The linear approach is nonetheless unable to capture the onset of transition and the curves continue smoothly beyond that point. In contrast, transition onset in the PSE case is characterized by a swift amplification of the modes at $Re_{\delta*} \approx 1120$.

5. Conclusion and outlook

An approach for the treatment of the laminar region in simulations of transitional flows was presented. The streamwise evolution of small disturbances in the laminar boundary layer is computed using the nonlinear parabolized stability equations. The concept is especially suited for wall-modeled large eddy simulations, which are an efficient tool in the study of fully turbulent flows but are unable to identify the onset of transition. It is not restricted to Blasius boundary layers and can also be applied in the presence of streamwise pressure gradients as well as in three-dimensional flows that give rise to inviscid cross-flow instabilities. In the next stage of this work, the practical viability of the concept will be evaluated by applying the PSE solution at the onset of the transition region as an inflow condition of a wall-modeled large eddy simulation.

REFERENCES

Bertolotti, F. P., Herbert, T. & Spalart, P. R. 1992 Linear and nonlinear stability of the Blasius boundary layer. *J. Fluid Mech.* **242**, 441–474.

Choi, H. & Moin, P. 2012 Grid-point requirements for large eddy simulation: Chapman's estimates revisited. *Phys. Fluids* **24**, 011702.

Day, M. J., Mansour, N. N. & Reynolds, W. C. 2001 Nonlinear stability and structure of compressible reacting mixing layers. *J. Fluid Mech.* **446**, 375–408.

Esfahanian, V., Hejranfar, K. & Sabetghadam, F. 2001 Linear and nonlinear PSE for stability analysis of the Blasius boundary layer using compact scheme. *J. Fluids Eng.* **123**, 545–550.

Haj-Hariri, H. 1994 Characteristics analysis of the parabolized stability equations. *Stud. Appl. Math.* **92**, 41–53.

Herbert, T. 1988 Secondary instability of boundary layers. *Ann. Rev. Fluid Mech.* **20**, 487–526.

Herbert, T. 1991 Boundary-layer transition - analysis and prediction revisited. *AIAA Paper* 91-0737.

Kachanov, Y. S. & Levchenko, V. Y. 1984 The resonant interaction of disturbances at laminar-turbulent transition in a boundary layer. *J. Fluid Mech.* **138**, 209–247.

Joslin, R. D., Streett, C. L. & Chang, C.-L. 1993 Spatial direct numerical simulation of boundary-layer transition mechanisms: Validation of PSE theory. *Theor. Comp. Fluid Dyn.* **4**, 271–288.

Park, G. I. & Moin, P. 2014 An improved dynamic non-equilibrium wall-model for large eddy simulation. *Phys. Fluids* **26**, 015108.

Sayadi, T., Hamman, C. W. & Moin, P. 2013 Direct numerical simulation of complete H-type and K-type transitions with implications for the dynamics of turbulent boundary layers. *J. Fluid Mech.* **724**, 480–509.

Sayadi, T. & Moin, P. 2012 Large eddy simulation of controlled transition to turbulence. *Phys. Fluids* **24**, 114103.

Schlichting, H. & Gersten, K. 2006 *Grenzschicht-Theorie*, 10th edn. Springer, Berlin Heidelberg New York.

Slotnick, J., Khodadoust, A., Alonso, J., Darmofal, D., Gropp, W., Lurie, E. & Mavriplis, D. 2014 CFD Vision 2030 study: A path to revolutionary computational aerosciences vision 2030 study: A path to revolutionary computational aerosciences. *Tech. Rep.* CR–2014-218178. NASA.